

ARE RED TIDAL FEATURES UNEQUIVOCAL SIGNATURES OF MAJOR DRY MERGERS?

DAISUKE KAWATA^{1,2}, JOHN S. MULCHAHEY¹, BRAD K. GIBSON³, AND PATRICIA SÁNCHEZ-BLÁZQUEZ⁴

Submitted to ApJ

ABSTRACT

We use a cosmological numerical simulation to study the tidal features produced by a minor merger with an elliptical galaxy. We find that the simulated tidal features are quantitatively similar to the red tidal features, i.e., dry tidal features, recently found in deep images of elliptical galaxies at intermediate redshifts. The minor merger in our simulation does not trigger star formation due to active galactic nuclei heating. Therefore, both the tidal features and the host galaxy are red, i.e. a dry minor merger. The stellar mass of the infalling satellite galaxy is about $10^{10} M_{\odot}$, and the tidal debris reach the surface brightness of $\mu_R \sim 27$ mag arcsec $^{-2}$. Thus, we conclude that tidal debris from minor mergers can explain the observed dry tidal features in ellipticals at intermediate redshifts, although other mechanisms (such as major dry mergers) may also be important.

Subject headings: galaxies: kinematics and dynamics — galaxies: formation — galaxies: stellar content

1. INTRODUCTION

Recently van Dokkum (2005, hereafter vD05) analyzed unprecedentedly deep image of red galaxies at redshift around $z \sim 0.1$, and found that they often have diffuse tidal features over the scale of ~ 50 kpc. Furthermore, there is no associated star formation with these tidal features. vD05 call such features “dry tidal features”. vD05 also find that 30 % of the red galaxies in their sample are undergoing *ongoing* mergers, and the luminosity difference of these merging galaxies are often small (the ratio of the luminosities between the bigger and smaller galaxies is more than 0.3). However, it is still an open question whether most dry tidal features are the remnants of such major dry mergers or whether other mechanisms can produce these features⁵.

Here, we show that deep images of simulated red galaxies also display red tidal features. The galaxy studied is taken from a fully self-consistent Λ -dominated cold dark matter (Λ CDM) cosmological simulation. We identify the responsible incident for the dry tidal feature, and find that the feature is due to the tidal tails created from an infall of a relatively small satellite galaxy, i.e. a minor merger. Our simulation suggests that such minor mergers may be responsible for some of the dry tidal features observed in vD05.

Our numerical simulations and the simulated elliptical galaxy are described in the next section. Section 3 presents a quantitative comparison between the dry tidal features in the simulated galaxy and those observed in vD05, and shows that the simulated features are consistent with the observed ones. The implications of this finding and our conclusions are given in the final section.

¹ The Observatories of the Carnegie Institution of Washington, 813 Santa Barbara Street, Pasadena, CA 91101

² Swinburne University of Technology, Hawthorn VIC 3122, Australia

³ Centre for Astrophysics, University of Central Lancashire, Preston, PR1 2HE, United Kingdom

⁴ Laboratoire d’Astrophysique, École Polytechnique Fédérale de Lausanne (EPFL) Observatoire, CH-1290, Sauverny, Switzerland

⁵ Throughout this paper, we call a merger whose luminosity ratio is greater than 0.3 “major merger”, and a merger whose luminosity ratio is less than 0.3 “minor merger”.

2. TARGET SIMULATED ELLIPTICAL GALAXY

The simulated images considered here are based on the elliptical galaxy model 2 presented in Kawata & Gibson (2005, hereafter KG05). KG05 carried out Λ CDM cosmological simulations using the galactic chemodynamics code, GCD+ (Kawata & Gibson 2003a). GCD+ is a three-dimensional tree N -body/smoothed particle hydrodynamics (SPH) code which incorporates self-gravity, hydrodynamics, radiative cooling, star formation, supernovae (SNe) feedback, and metal enrichment. GCD+ takes account of the chemical enrichment by both Type II (SNe II) and Type Ia (SNe Ia) SNe, mass-loss from intermediate mass stars, and follows the chemical enrichment history of both the stellar and gas components of the system.

The cosmological simulation adopts a Λ CDM cosmology ($\Omega_0=0.3$, $\Lambda_0=0.7$, $\Omega_b=0.019h^{-2}$, $h=0.7$, and $\sigma_8=0.9$), and uses a multi-resolution technique to achieve high-resolution in the regions of interest, including the tidal forces from neighboring large-scale structures. The initial conditions for the simulations are constructed using the public software GRAFIC2 (Bertschinger 2001). Gas dynamics and star formation are included only within the relevant high-resolution region (~ 12 Mpc at $z=0$); the surrounding low-resolution region (~ 43 Mpc) contributes to the high-resolution region only through gravity. Consequently, the initial condition consists of a total of 190093 dark matter particles and 134336 gas particles. The mass and softening lengths of individual gas (dark matter) particles in the high-resolution region are 5.86×10^7 (3.95×10^8) M_{\odot} and 2.27 (4.29) kpc, respectively.

The elliptical galaxy found by KG05 (see also Kawata & Gibson 2003b) has a total virial mass of $2 \times 10^{13} M_{\odot}$. The galaxy is relatively isolated, with only a few low-mass satellites remaining at $z=0$. Figure 1 of Kawata & Gibson (2003b) shows the morphological evolution of dark matter in the simulation volume and the evolution of the stellar component of the target galaxy. The galaxy forms through conventional hierarchical clustering between redshifts $z=3$ and $z=1$. The morphology has not changed dramatically since $z=1$.

KG05 introduced an active galactic nuclei (AGN) heating model in the simulation, and found that self-regulated activity of the AGN can suppress significant late-time star formation – characteristics not encountered in traditional dynamical models of ellipticals. As a result, their model (model 2 of KG05) succeeds in reproducing both the observed X-ray and optical properties of a massive elliptical galaxy.

In the chemodynamical simulation, the simulated star particles each carry their own age and metallicity “tag”, which enables us to generate an optical-to-near infrared spectral energy distribution for the simulated galaxy, when combined with our population synthesis code (which itself is based upon the population synthesis models of Kodama & Arimoto 1997). The population synthesis models are used to construct the photometric images used in our analysis.

3. DRY TIDAL FEATURES IN THE TARGET GALAXY

Figures 1-4 show the morphological evolution of the target galaxy over the redshift range $z = 0.4$ to $z = 0.22$ at two different projections: $x - y$ and $x - z$ projection in our three dimensional simulation coordinate system. The top and middle panels in each figure show the deep ($R < 27.0$ mag arcsec $^{-2}$) and shallow ($R < 24.5$ mag arcsec $^{-2}$) images, respectively. The deep images reveal some small tidal features which are not visible in the shallow images. The tidal features are similar to some of the diffuse tidal tail like features which are observed in vD05, e.g., 5-994, 9-360, 10-232, 16-650, 16-1302, 17-2819, 21-523, 25-3572 in his sample. For example, in Figure 1, the panels at $z = 0.37, 0.34$, and 0.32 show faint features like tidal tails. In fact, these are the tidal tails of a small satellite infalling into the target galaxy. The infalling satellite galaxy is highlighted by the circle in the top-left panel of Figures 1 and 2. The bottom panels show the distribution of the star particles. The grey dots show the whole particles, while the black dots represent the particles originated from the infalling satellite. The satellite particles are defined as the particles whose radius from the center of the satellite is less than 20 kpc at $z = 0.45$, well before the satellite falls into the target galaxy. The figures show that the tidal features seen in the deep R -band image correspond to the tidal tails of the infalling satellite. The tidal tails of the satellite start to be developed at $z = 0.40$. The satellite is tidally disrupted at $z = 0.37$, and the tidal features disappear around $z = 0.25$, which corresponds to about 1.3 Gyr. During the period when the tidal tails are visible in the bottom panels, the tidal features also appear in the deep image, although, not surprisingly, the strength of the features depends on the projection angle. vD05 claims that the tidal features appear smooth, showing little or no evidence for clumps and condensations. On the other hand, the simulated tidal features suggest the appearance of small clump prior to redshift $z=0.34$, when the satellite has yet to fully disrupt. However, one can appreciate from Figure 11 of vD05 that some fraction of the observed galaxies present tidal tail-like features accompanied with small clumps, for example galaxies 9-360, 10-232, 17-2819, and 21-523. They may be an early stage of a minor merger. After redshift $z=0.34$, there are appear to be no discernible condensations in the tidal tails.

Another important aspect reported in vD05 is that both the host galaxy and the tidal features are red, and there is no sign of star formation, i.e., they are “dry”. Similarly, in our simulation the produced features are in fact “dry tidal features”. Figure 5 shows the history of the star formation rate of the system, replotted from Figure 3 of KG05. Star formation stops in the target galaxy just before $z \sim 0.4$, due to the AGN heating (see KG05 for details). The AGN heating also suppresses star formation during the infall of the satellite galaxy.

Table 1 displays the luminosity, colors, and mass of the target galaxy and the infalling satellite at $z = 0.4$, i.e., before they start merging. Here, we adopt the diameter of $D = 5$ arcsec for a comparison with vD05. The stellar mass ratio between the satellite galaxy and the target galaxy is about 0.03, which indicates that the infalling satellite is small, i.e., a minor merger. This indicates that dry tidal features can result from minor mergers.

Table 1 gives two values for the luminosity of the target galaxy: One is the total luminosity, while the second value is the luminosity when the contribution from stars which are younger than 3 Gyr is ignored. Since star formation stops just before $z = 0.4$ in the target galaxy, the luminosity at $z = 0.4$ is affected by some young stars. As argued in KG05, this late cessation of star formation in the simulated galaxy is due to our simple modeling of the AGN heating. In this simulation, the AGN heating was started at $z = 1$, which is likely too late. If the AGN heating is added at a higher redshift, star formation is expected to stop earlier. For real elliptical galaxies, the epoch of the termination of star formation is expected to be rather random, and objects detected as red elliptical galaxies are likely at a stage well after star formation ceases (e.g., Shioya & Bekki 1998; van Dokkum & Franx 2001). Thus, the luminosity when the young stellar population is ignored is more appropriate for objects selected to be red and this is the luminosity we consider here. For such an object, the luminosity difference, $L_1/L_2 = 10^{(M_{R,1}-M_{R,2})/2.5}$, between the target galaxy and the satellite galaxy is 0.05, which is consistent with the lowest luminosity ratios found in the sample of ongoing mergers in vD05. In fact, those galaxies, 1-2874 and 5-2345 in vD05, show clear tidal tails, like those seen at $z = 0.37$ in Figure 1. Table 1 also shows the colors for both the target galaxy and the satellite, which indicates that they are both red, and the difference in $B - R$ is 0.14. This color difference is driven by the difference in metallicity.

Figure 6 shows the evolution of the luminosity and colors of the target galaxies. The filled circles indicate the colors and magnitudes before $z = 0.2$, when we found the dry tidal features. The open circles represent the evolution at later stages. The area enclosed by the dotted lines indicates the selection criteria in vD05. As discussed in vD05, their selection criteria preferably selects red galaxies at $z < 0.2$. The epoch we focus on here is a little earlier, and the target galaxy is redder than the selection criterion adopted by vD05. However, the epoch of minor mergers is random, and such minor mergers are expected to happen often in a Λ CDM cosmology. Hence, the results presented here indicate that if minor mergers happen at $z < 0.2$ for elliptical galaxies, the dry tidal features observed in vD05 can be produced.

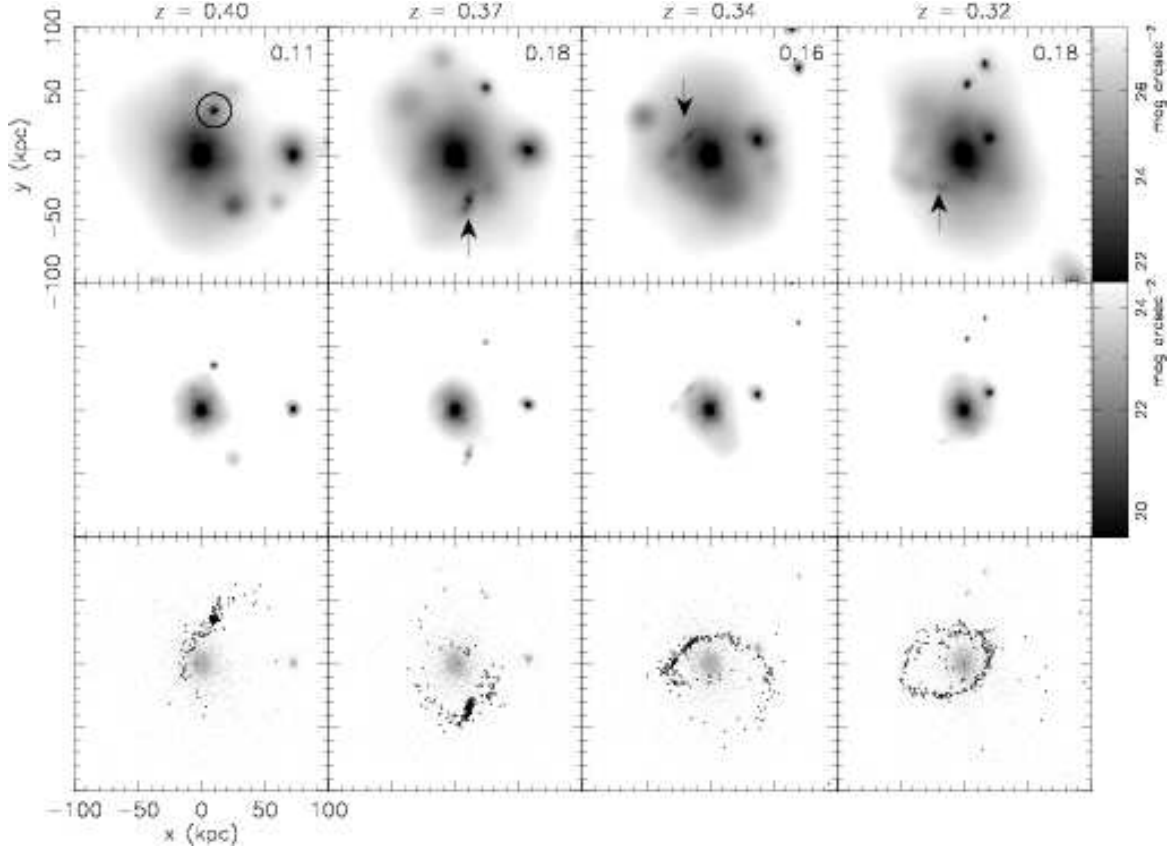


FIG. 1.— Deep (upper panels) and shallow (middle panels) predicted *R*-band images of the target galaxy at the $x - y$ projections over the redshift range $z = 0.4$ to $z = 0.32$. Bottom panels represent the distributions of star particles (gray dots), the particles within the infalling satellite (see text for details) are highlighted by black dots. The infalling satellite galaxy is highlighted by the circle in the top-left panel. The prominent features are indicated by arrows. Numbers shown in the top panels are the tidal parameter, t , (see text) for each image.

TABLE 1
THE LUMINOSITY, COLOR, AND MASS OF THE TARGET GALAXY AND THE INFALLING
SATELLITE AT $z = 0.4^a$.

the target galaxy				the satellite		
M_R (mag)	M_R (age>3 Gyr) ^b (mag)	$B - R^c$	M_* (M_\odot)	M_R (mag)	$B - R$	M_* (M_\odot)
-23.25	-22.50	2.53	3.1×10^{11}	-19.17	2.39	1.0×10^{10}

^aThe luminosity is measured within the projected diameter of 5 arcsec, i.e. 26.7 kpc at $z = 0.4$, while the mass is measured within the three dimensional diameter of 26.7 kpc.

^bThe *R*-band luminosity, when the contribution from the stars younger than 3 Gyr is ignored.

^cThe color, when the contribution from the stars younger than 3 Gyr is ignored.

Finally, we quantitatively confirm that the tidal features shown here are consistent with the features observed in vD05. To this end, we have analyzed the tidal parameter, t , which is defined in Section 5.3 in vD05, for all the *R*-band images presented in Figures 1-4. Here, we briefly explain our procedures to obtain the tidal parameter. We refer to the simulated galaxy *R*-band image as “ G ”. First, the galaxy images are fit by an elliptical model using the `ellipse` task in IRAF. The center position, ellipticity, and position angle are allowed to vary with radius. In cases where there are galaxies which overlap with the target galaxy in projection, the overlapping objects are also fit. The final model image is indicated

by “ M ”. Finally, a fractional distortion image, “ F ”, is created by dividing G by M . When the pixel value of F is defined by $F(x, y)$, and the mean value of the image is \overline{F} , the tidal parameter t which describes the level of distortion is defined as $t = \overline{F(x, y) - \overline{F}}$. Figure 7 demonstrates this procedure.

The values of t are shown in all the top panels in Figures 1-4. We can see that the *R*-band images which have the tidal features show higher t value ($t > 0.1$). During the epoch when the tidal features of the satellite galaxy are visible in the bottom panels ($z > 0.25$), t appears to be higher. As expected, the t values are lower after the tidal features disappear at $z \sim 0.25$. We also find that

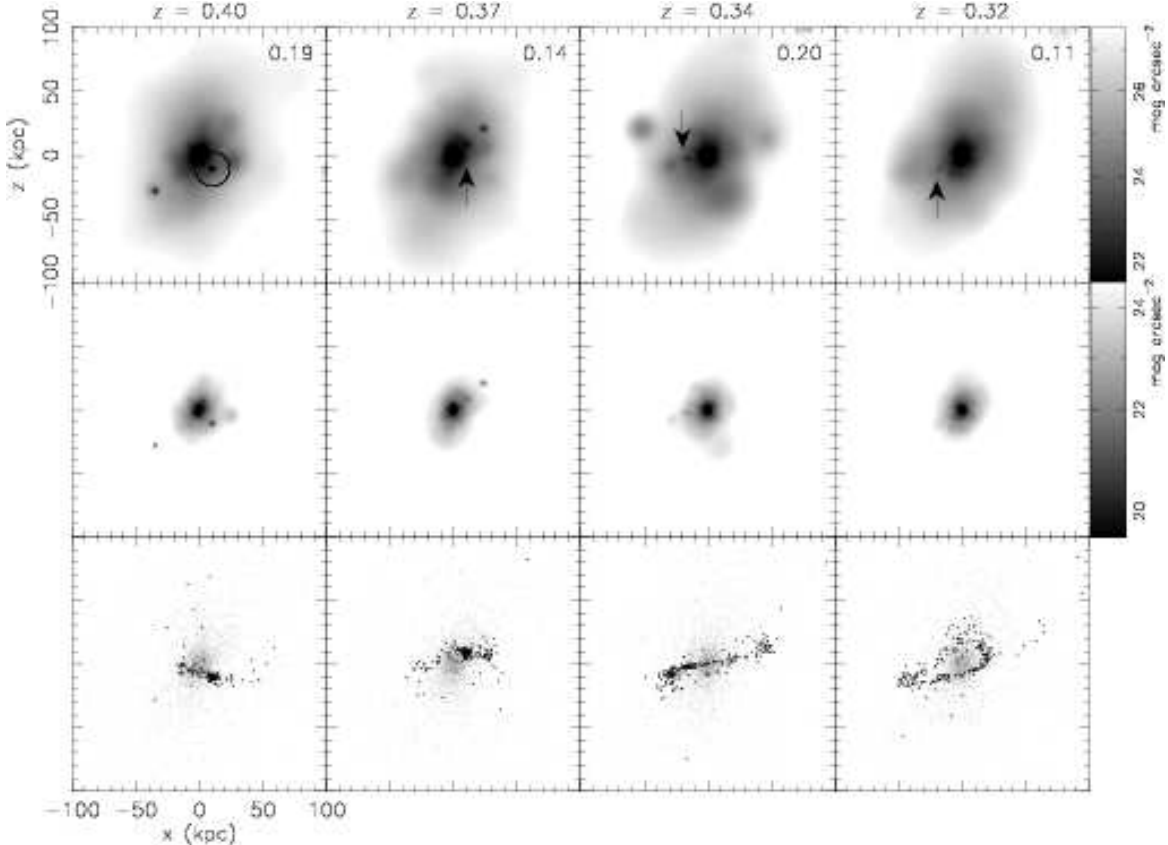


FIG. 2.— Same as Figure 1, but for the $x - z$ projections. The high value of the tidal parameter at $z = 0.4$ is caused by poor model subtraction due to the small separation between the target galaxy and the infalling satellite.

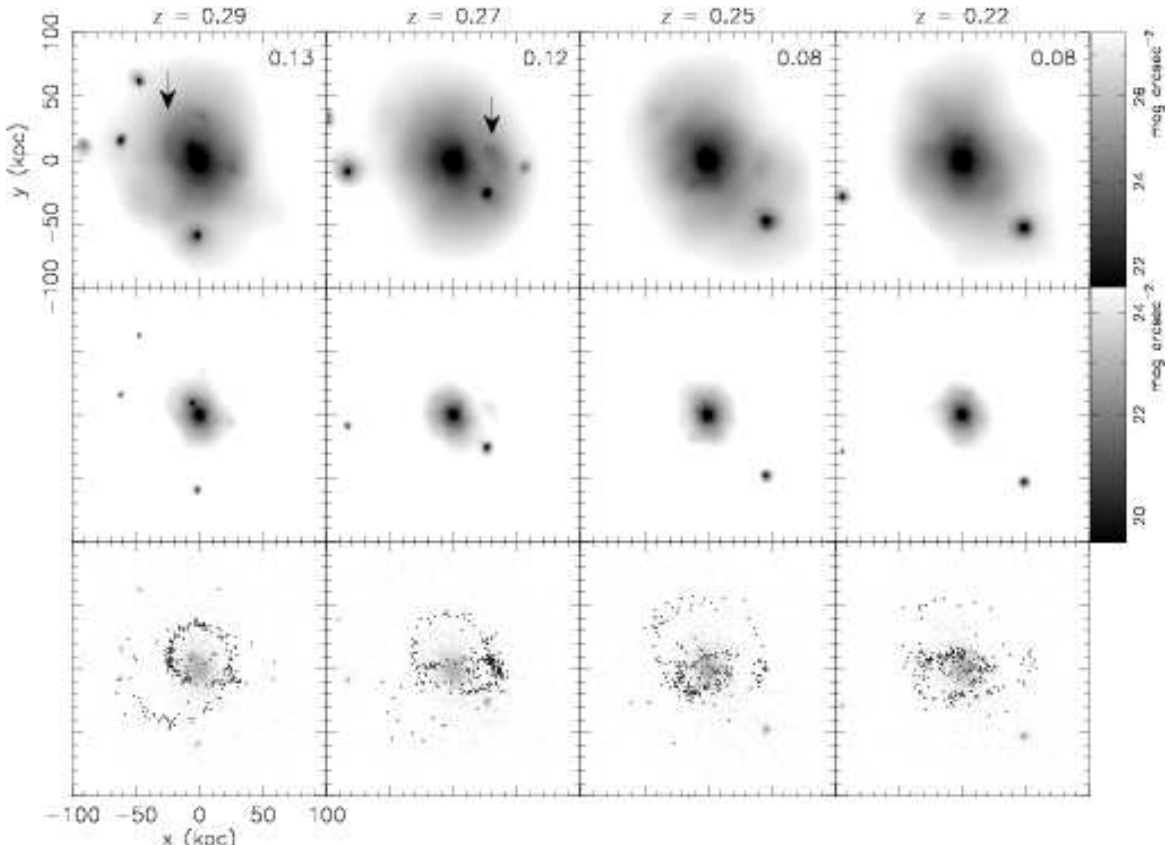


FIG. 3.— Same as Figure 1, but for redshift range $z = 0.29$ to $z = 0.22$. In some cases, the different projections give vastly different t values (com-

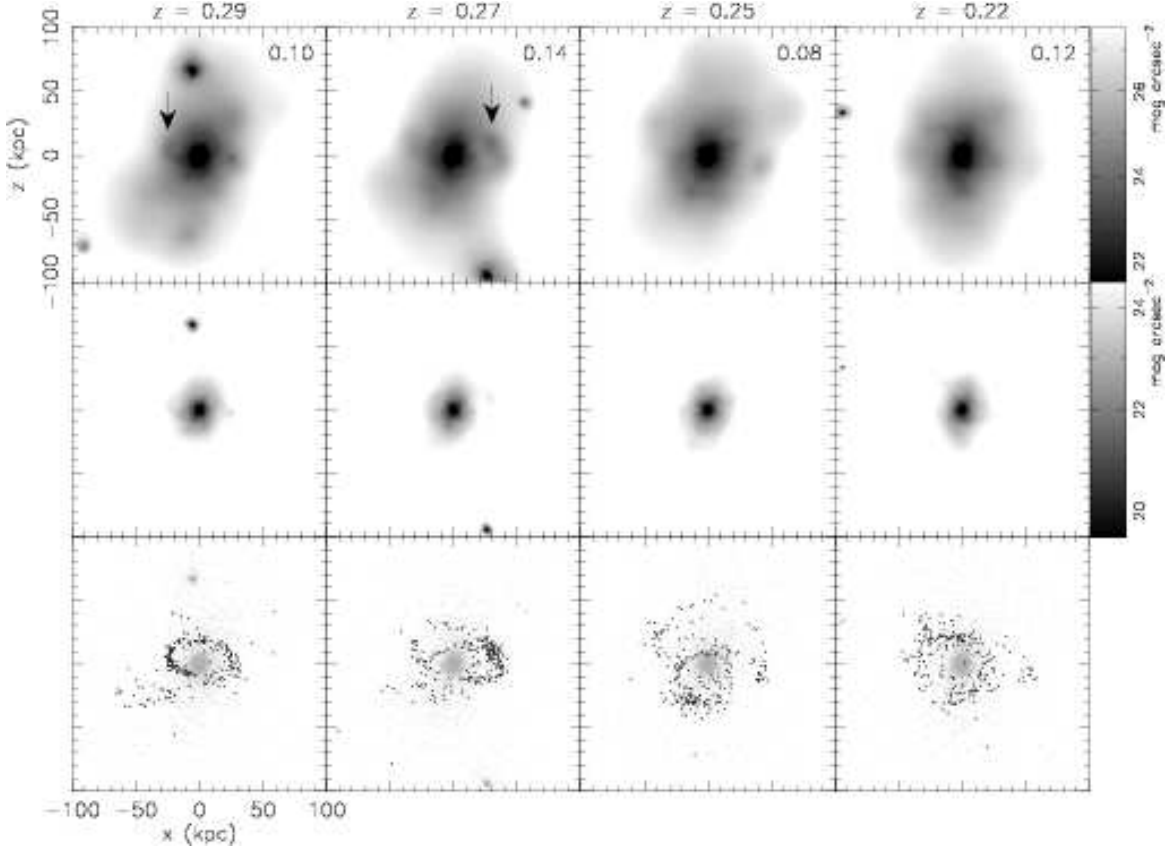


FIG. 4.— Same as Figure 3, but for the $x - z$ projections.

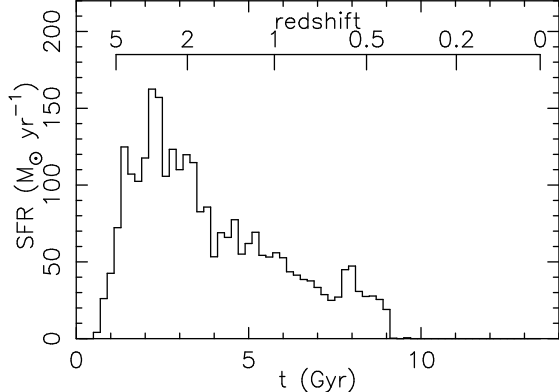


FIG. 5.— Time-variation of the star formation rate for the target galaxy.

pare for example the $x - y$ and $x - z$ panels at $z = 0.32$.

The range of t values is consistent with the weakly (median value of t is 0.13 in vD05) and strongly (median $t = 0.19$) disturbed galaxies classified in vD05. Thus, quantitatively we confirm that the dry tidal features seen in our simulated galaxies are consistent with the dry tidal features seen in vD05.

4. DISCUSSION AND CONCLUSIONS

We have demonstrated that a minor merger of a satellite galaxy whose stellar mass is $10^{10} M_\odot$ with a massive elliptical galaxies can produce dry tidal features. In the present simulation, the features last about 1.3 Gyr, although the lifetime of such features must depend on the orbit of the satellite galaxy. Traditionally cosmological numerical simulations of ellip-

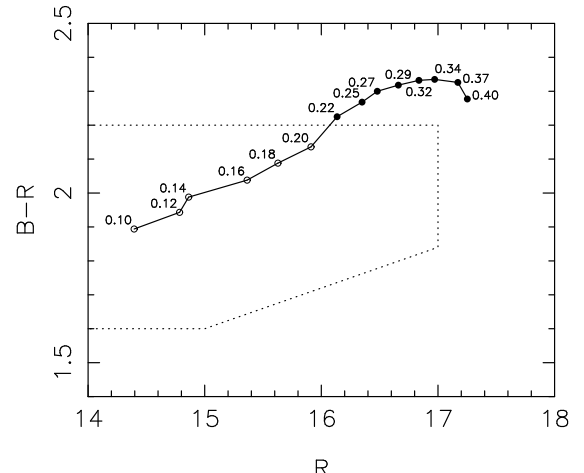


FIG. 6.— Time variation of $B - R$ color and the R -band magnitude for the target galaxy. The numbers indicate redshift. The filled circles are the colors and magnitudes before $z = 0.2$, which we focus on in this paper. The open circles present the evolution after the stages which are discussed in this paper. The area enclosed by the dotted lines are the selection criteria in vD05.

tical galaxy formation have suffered from an inability to suppress late-time star formation in the simulation (e.g., Sugimohara & Ostriker 1998; Lewis et al. 2000; Kay et al. 2003; Tornatore et al. 2003; Meza et al. 2003; Kawata & Gibson 2003b; Borgani et al. 2004), thereby being inconsistent with the observed red color in bright elliptical galaxies. However, self-regulated AGN heating, of the sort introduced in KG05 aids in the suppression of late-time star formation. As a result, both the host galaxy and tidal features in our simulation have the red

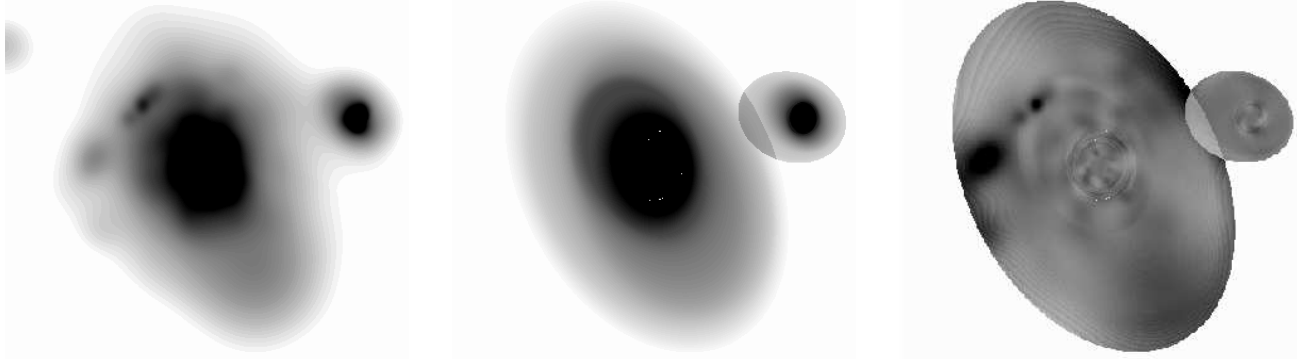


FIG. 7.— Demonstration of the process to derive the value of the tidal parameter, t (see text for the details). Left panel shows the R -band image; middle panel is the elliptical model; right panel presents the distortion image.

colors consistent with those observed by vD05.

In a Λ CDM cosmology, minor mergers as seen in our simulations are expected to happen much more frequently than major mergers. This might explain the high detection rate of tidal features in vD05. In addition, minor mergers are consistent with the red features observed, because mergers with a small galaxy have a relatively weak effect on the inter-stellar medium (ISM) of the host galaxy. On the other hand, major mergers must have a stronger effect on the ISM even for elliptical galaxies, where the system is likely to suffer from radiative cooling. This in turn likely induces star formation, resulting in blue galaxy colors. However, some dry tidal features should be produced from major mergers, as long as these mergers are also "dry". In fact, ongoing dry major mergers are observed at various redshifts below $z=1$ (e.g., vD05; Tran et al. 2005; Bell et al. 2006), and it is known that such major dry mergers can create tidal features (e.g., Combes et al. 1995; Bell et al. 2006). In addition, such major dry mergers do not violate the scaling relations of elliptical galaxies (e.g., Naab et al. 2006; Boylan-Kolchin et al. 2005, 2006). Our results should not be interpreted as degrading the importance of major dry mergers, but instead that dry tidal features do not necessarily derive from a major dry merger and that a viable alternate pathway for their appearance may be that of a minor dry merger. In other words, infalling galaxies over a wide range of mass may be responsible for producing the observed dry tidal features in elliptical galaxies. Therefore, considerable caution is needed to use the dry tidal features for estimates of the major dry merger rate. Note that vD05 carefully estimates the major dry merger rate, taking into account only the sample of ongoing dry major mergers.

Johnston et al. (2001) demonstrate that if the infalling galaxy was a dwarf spheroidal with the mass of $\sim 10^8 M_\odot$, like seen in the Local Group, the surface brightness of the tidal debris would be lower than $\mu_R \sim 28$ mag arcsec $^{-2}$ after the dwarf is well-disrupted. Thus, mergers with the most common low mass galaxies are apparently not sufficient to produce the features found by vD05. Since the infalling galaxy in our simulation has a stellar mass of $10^{10} M_\odot$, the surface brightness of the resulting tidal debris is much higher, making the features detectable at the depths achieved in vD05. Hence, the dry tidal features observed in vD05 are expected to

be end-products of mergers with a system whose stellar mass is at least $\sim 10^{10} M_\odot$. Systematic studies like that of Johnston et al. (2001), but with higher mass satellites, would be useful for determining the mass range required to reproduce the observed dry tidal features.

The mechanism which creates the dry tidal feature in our simulation is similar to what is suggested for the formation of ripples (Schweizer 1980) and shells (Malin & Carter 1980) observed in nearby elliptical galaxies (e.g., Schweizer & Seitzer 1992; Colbert et al. 2001). Previous studies demonstrate that both a major (e.g., Hernquist & Spergel 1992) and minor (e.g., Quinn 1984; Dupraz & Combes 1986; Hernquist & Quinn 1988; Kojima & Noguchi 1997) merger can create shell features around giant elliptical galaxies. vD05 claims that their dry tidal features are different from the ripples and shells seen in nearby elliptical galaxies, because the dry tidal features look smoother than these other structures. However, vD05 also notes that the resolution of his images make it difficult to reach strong conclusions about the differences between these various types of features. According to the previous systematic studies of minor mergers (e.g., Hernquist & Quinn 1988), smoother features are produced if the infalling galaxy is more of a velocity dispersion supported system, i.e., elliptical galaxies. In addition, the tidal features are sensitive to the infall orbit, and the previous simulations demonstrate that off-center infall can create large scale features around the host galaxy. The infalling galaxy seen in our simulation has an off-center orbit, and thus creates the tidal features over a large scale, ~ 50 kpc in radius.

The dry major merger is considered to be an important mechanism because one major merger is enough to explain the observed factor of two increase in stellar mass in bright red galaxies since redshift $z=1$ (Bell et al. 2004; Faber et al. 2005). It is an important question whether or not minor mergers, such as those described here, can similarly contribute to the increase in the mass of bright red galaxies. To check this, we compared the stellar mass of the simulated galaxy within a radius of 100 kpc at $z=1$ and $z=0$. As mentioned above, the simulated galaxy suffers from an excess of ongoing late-time star formation (prior to $z \sim 0.4$ – see also Fig. 5). Hence, we exclude stars whose age at the present epoch is less than 8 Gyrs. As a result, we find little increase in stellar mass subsequent to $z=1$ (less than 5% growth). This is because the

simulated galaxy does not undergo a major merger subsequent to redshift $z = 1.5$, and the disrupted satellites are much less massive than the host galaxy. (Note that in Table 1 we measure the stellar mass within a small aperture and therefore underestimate the total stellar mass of the host galaxy.) Therefore, minor mergers such as those described here are unlikely to contribute to the observed mass evolution of red galaxies. This means that major dry mergers must occur for a significant fraction of the red galaxy population, although we emphasise again that while potentially the dominant evolutionary pathway, it is not a mutually exclusive one. Interestingly, Kong et al. (2006) claim that the stellar mass increase is important for the relatively faint early-type galaxies (see also Renzini 2006). There may be a mass dependence of the dry major merger rate.

Our simulations of a single elliptical galaxy leaves many open questions. For example, how often do mi-

nor mergers happen for bright elliptical galaxies and how do the resulting features depend on the mass and morphology of the infalling galaxy. To address these questions, simulations of a large sample of ellipticals will be required.

DK thanks the financial support of the JSPS, through Postdoctoral Fellowship for research abroad. The Australian Research Council, through its Discovery Project scheme, is gratefully acknowledged. We acknowledge the Yukawa Institute Computer Facility, the Astronomical Data Analysis Center of the National Astronomical Observatory, Japan (project ID: wmn14a), the Institute of Space and Astronautical Science of Japan Aerospace Exploration Agency, and the Australian and Victorian Partnerships for Advanced Computing, where the numerical computations for this paper were performed.

REFERENCES

- Bell, E. F., Naab, T., McIntosh, D. H., Somerville, R. S., Caldwell, J. A. R., Barden, M., Wolf, C., Rix, H.-W., Beckwith, S. V., Borch, A., Häussler, B., Heymans, C., Jahnke, K., Jogee, S., Koposov, S., Meisenheimer, K., Peng, C. Y., Sanchez, S. F., & Wisotzki, L. 2006, *ApJ*, 640, 241
- Bell, E. F., Wolf, C., Meisenheimer, K., Rix, H.-W., Borch, A., Dye, S., Kleinheinrich, M., Wisotzki, L., & McIntosh, D. H. 2004, *ApJ*, 608, 752
- Bertschinger, E. 2001, *ApJS*, 137, 1
- Borgani, S., Murante, G., Springel, V., Diaferio, A., Dolag, K., Moscardini, L., Tormen, G., Tornatore, L., & Tozzi, P. 2004, *MNRAS*, 348, 1078
- Boylan-Kolchin, M., Ma, C.-P., & Quataert, E. 2005, *MNRAS*, 362, 184
- . 2006, ArXiv Astrophysics e-prints
- Colbert, J. W., Mulchaey, J. S., & Zabludoff, A. I. 2001, *AJ*, 121, 808
- Combes, F., Rampazzo, R., Bonfanti, P. P., Pringniel, P., & Sulentic, J. W. 1995, *A&A*, 297, 37
- Dupraz, C., & Combes, F. 1986, *A&A*, 166, 53
- Faber, S. M., Willmer, C. N. A., Wolf, C., Koo, D. C., Weiner, B. J., Newman, J. A., Im, M., Coil, A. L., Conroy, C., Cooper, M. C., Davis, M., Finkbeiner, D. P., Gerke, B. F., Gebhardt, K., Groth, E. J., Guhathakurta, P., Harker, J., Kaiser, N., Kassin, S., Kleinheinrich, M., Konidaris, N. P., Lin, L., Luppino, G., Madgwick, D. S., Noeske, K. M. K. G., Phillips, A. C., Sarajedini, V. L., Simard, L., Szalay, A. S., Vogt, N. P., & Yan, R. 2005, ArXiv Astrophysics e-prints
- Hernquist, L., & Quinn, P. J. 1988, *ApJ*, 331, 682
- Hernquist, L., & Spergel, D. N. 1992, *ApJ*, 399, L117
- Johnston, K. V., Sackett, P. D., & Bullock, J. S. 2001, *ApJ*, 557, 137
- Kawata, D., & Gibson, B. K. 2003a, *MNRAS*, 340, 908
- . 2003b, *MNRAS*, 346, 135
- . 2005, *MNRAS*, 358, L16
- Kay, S. T., Thomas, P. A., & Theuns, T. 2003, *MNRAS*, 343, 608
- Kodama, T., & Arimoto, N. 1997, *A&A*, 320, 41
- Kojima, M., & Noguchi, M. 1997, *ApJ*, 481, 132
- Kong, X., Daddi, E., Arimoto, N., Renzini, A., Broadhurst, T., Cimatti, A., Ikuta, C., Ohta, K., da Costa, L., Olsen, L. F., Onodera, M., & Tamura, N. 2006, *ApJ*, 638, 72
- Lewis, G. F., Babul, A., Katz, N., Quinn, T., Hernquist, L., & Weinberg, D. H. 2000, *ApJ*, 536, 623
- Malin, D. F., & Carter, D. 1980, *Nature*, 285, 643
- Meza, A., Navarro, J. F., Steinmetz, M., & Eke, V. R. 2003, *ApJ*, 590, 619
- Naab, T., Khochfar, S., & Burkert, A. 2006, *ApJ*, 636, L81
- Quinn, P. J. 1984, *ApJ*, 279, 596
- Renzini, A. 2006, ArXiv Astrophysics e-prints
- Schweizer, F. 1980, *ApJ*, 237, 303
- Schweizer, F., & Seitzer, P. 1992, *AJ*, 104, 1039
- Shioya, Y., & Bekki, K. 1998, *ApJ*, 504, 42
- Suginohara, T., & Ostriker, J. P. 1998, *ApJ*, 507, 16
- Tornatore, L., Borgani, S., Springel, V., Matteucci, F., Menci, N., & Murante, G. 2003, *MNRAS*, 342, 1025
- Tran, K.-V. H., van Dokkum, P., Franx, M., Illingworth, G. D., Kelson, D. D., & Schreiber, N. M. F. 2005, *ApJ*, 627, L25
- van Dokkum, P. G. 2005, *AJ*, in press (astro-ph/0506661),
- van Dokkum, P. G., & Franx, M. 2001, *ApJ*, 553, 90